Food Chemistry: X 25 (2025) 102240

Contents lists available at ScienceDirect

Food Chemistry: X

journal homepage: www.sciencedirect.com/journal/food-chemistry-x

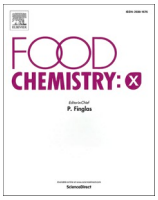

The transport of polyphenols from *Camellia fascicularis* in Caco-2 cells based on UPLC-ESI-MS/MS

Shengjiang Duan [a,1], Hao Zheng [a,1], Junrong Tang [b], Huan Kan [a,b], Changwei Cao [a,b,*], Zhijiao Shi [a,*], Yun Liu [a,b,*]

[a] College of Biological Science and Food Engineering, Southwest Forestry University, Kunming 650224, China
[b] Forest Resources Exploitation and Utilization Engineering Research Center for Grand Health of Yunnan Provincial Universities, Southwest Forestry University, Kunming 650224, China

ARTICLE INFO

Keywords:
Camellia fascicularis
Polyphenols
Caco-2 cells
Transport
Metabolites

ABSTRACT

Camellia fascicularis, as a food and medicinal plant, is rich in polyphenols. Herein, digestion samples (DS) of *C. fascicularis* polyphenols (CFPs) were metabolically analyzed based on their bidirectional translocation in Caco-2 cells using ultraperformance liquid chromatography-electrospray ionization-tandem mass spectrometry. The results indicated that after DS transported via Caco-2 cell monolayer models nine polyphenol compounds in transit solution (TSB) from apical (AP) to basolateral (BL) side were upregulated, whereas seven in the transit solution (TSA) from BL to AP side were upregulated. In addition, 53 significantly different polyphenol compounds dominated by flavonoids were identified in the TSA vs. TSB groups, with a dominantly moderate degree of uptake. Among them, 40 polyphenol compounds were upregulated including eupatorin, 5,7,4′-trihydroxy-3,6,3′,5′-tetramethoxyflavone, and jaceosidin-7-*O*-glucoside, which might exhibit active transport, whereas the remaining 13 were downregulated and might exhibit passive diffusive transport. This study offers a rationale that further explored the bioactive mechanisms of CFPs.

1. Introduction

Camellia fascicularis, which comes from genus *Camellia* in family Theaceae, is endemic to Yunnan Province, China. *C. fascicularis* is characterized by golden-yellow petals and is rich in carbohydrates, amino acids, minerals, and vitamins, providing remarkable ornamental and nutritional value (Liu et al., 2019; Peng et al., 2022). Moreover, *C. fascicularis* contains a variety of biologically active substances like polyphenols, flavonoids, polysaccharides, and saponins that exert antioxidant, anti-inflammatory, anti-tumor, and antibacterial benefits (Gao et al., 2022; Peng et al., 2022; Tang et al., 2024). The polyphenol content in *C. fascicularis* is higher than that of the other active ingredients and has been reported to be a major contributor to its anti-inflammatory benefits (Gao et al., 2022).

Plant polyphenols have been recognized as active substances that are beneficial to human health and can be categorized as phenolic acids, flavonoids, stilbenes, and lignans (Yang, Dong, Fang, Li, & Li, 2024). However, polyphenols vary in their content and type, leading to differences in their digestion and uptake by intestines. Relevant research indicated that some polyphenols may be directly absorbable by the small intestine. However, most polyphenols have complex chemical structures or interact with macromolecules in the plant matrix and are thus more difficult to absorb (Hlel et al., 2018). Polyphenols are readily absorbed by the body only after they are digested by the intestine into small molecules, thus enhancing their activity (Rocchetti, Chiodelli, Giuberti, & Lucini, 2018). The leaves of *C. fascicularis* have been reported to be rich in polyphenols, and relevant studies have focused on the isolation and purification of polyphenols, identification of their components, and their pharmacological effect (Gao et al., 2022; Liu et al., 2019). To date, the uptake and transport processes of polyphenols derived from *C. fascicularis* remain unclear.

Intestinal tract is the main site for the absorption of active substances and nutrients in humans. The structural properties and physiological functions of Caco-2 cell monolayer models are like small intestinal epithelial cells, therefore, it could be used to research the uptake and transport of active substances (Xiao et al., 2024). Recently, Caco-2 cell

* Corresponding authors at: College of Biological Science and Food Engineering, Southwest Forestry University, Kunming 650224, China.
E-mail addresses: ccwylf1111@swfu.edu.cn (C. Cao), shizhijiao@swfu.edu.cn (Z. Shi), liuyun@swfu.edu.cn (Y. Liu).
[1] These authors contributed equally to this work.

https://doi.org/10.1016/j.fochx.2025.102240
Received 14 November 2024; Received in revised form 15 January 2025; Accepted 24 January 2025
Available online 26 January 2025

monolayer models have been successfully constructed to evaluate the transport and utilization of active ingredients from drugs or food, such as curcumin, naringin, avenanthramides, caffeic acid, and ferulic acid (Chen, Li, Chen, Wang, & Luo, 2020; Faralli, Shekarforoush, Ajalloueian, Mendes, & Chronakis, 2018; Zhang et al., 2022). *C. fascicularis* is an important polyphenol-rich plant. In order to gain a more comprehensive understanding of the intestinal transport capacity of polyphenols from *C. fascicularis*, the Caco-2 cell monolayer model was selected to investigate their absorption and transport.

Herein, ultraperformance liquid chromatography-electrospray ionization-tandem mass spectrometry (UPLC-ESI-MS/MS) was used to analyze the *C. fascicularis*-derived polyphenols based on their bidirectional transport in Caco-2 cell monolayer models. Moreover, possible transit modes involved in the bidirectional transit of some polyphenols were explored. This research could offer foundation to further understand the uptake and transport mechanisms of digestion samples (DS) from *C. fascicularis* polyphenols (CFPs) and provide rationale for the exploitation of CFPs-based products.

2. Materials and methods

2.1. Materials and reagents

C. fascicularis leaves were harvested in March 2023 from Hekou County, Yunnan Province, China, and the CFPs produced as previously depicted by Liu et al. (2019). Specifically, the defatted powder of *C. fascicularis* leaves was microwaved in 50 % ethanol (1:32 g/mL) at 160 W for 20 s. The crude CFPs were collected and purified by using an HP-20 microporous adsorbent resin, and the purified solution then concentrated and freeze-dried to obtain CFPs.

Caco-2 cells were acquired from the Cell Bank of the Chinese Academy of Sciences (Shanghai, China). Dulbecco's modified Eagle's medium (DMEM), Hank's balanced salt solution (HBSS), phosphate-buffered saline, fetal bovine serum (FBS), penicillin–streptomycin solution (PS), alkaline phosphatase (AKP) kit, 6-well Transwell cell culture dish (Model 14,112, 24 mm membrane diameter, 0.4 μm pore size polyester membrane), Cell Counting Kit-8 (CCK-8), trypsin, and phenol red were provided by Nanjing Yifeixue Biotechnology Co., Ltd. (Nanjing, China). Folin–Ciocalteu reagent and gallic acid were obtained from Shanghai Yuanye Bio-Technology Co., Ltd. (Shanghai, China).

2.2. Preparation of digestion samples

DS were produced by approach from Brodkorb et al. (2019) with appropriate modifications. Specifically, 40 mg CFPs were solubilized in 5 mL purified water, and 3.5 mL simulated salivary solution and 0.5 mL α-amylase (1500 U/mL) were added, followed by 25 μL $CaCl_2$ (0.3 mol/L) and 0.5 mL purified water, which were then mixed thoroughly to simulate oral digestion for 2 min. Then, 7.5 mL simulated gastric solution and 1.6 mL pepsin (25,000 U/mL) were added, followed by 5 μL $CaCl_2$ (0.3 mol/L) and 0.15 mL HCl (1 mol/L), and the pH set to 3.0, followed by the addition of purified water to ensure a final volume up to 20 mL. After simulated gastric digestion for 2 h, 11 mL simulated intestinal fluid, 5 mL trypsin (800 U/mL), 2.5 mL bile salt (0.16 mmol/L), 40 μL $CaCl_2$ (0.3 mol/L), 0.15 mL NaOH (1 mol/L), and 1.31 mL purified water were added and mixed thoroughly to simulate intestinal digestion for 2 h. All the digestion processes were performed in a constant temperature shaker (SHZ-82, ZBR Instrument Manufacturing Co., Ltd., Jiangsu, China) at 37 °C and a rotational speed of 120 rpm, and the digested samples subjected to a boiling water bath, filtered, freeze-dried, and stored for further use.

2.3. Caco-2 cell monolayer modeling

The Caco-2 cell monolayer model was constructed following the methods by Taboada-López et al. (2021). After passaging, the cells were added to 5–6 mL complete medium (DMEM with 20 % FBS and 1 % PS) and cultured in an incubator (WCI-180, Thermo Fisher Scientific, Waltham, MA, USA) at 37 °C with 5 % CO_2.

Caco-2 cells in logarithmic growth phase were selected and digested with1.0 mL trypsin for 2 min. After centrifugation and removal of the supernatant, complete medium was added and resuspended. Caco-2 cells at a density of 1×10^6 cells/mL were then inoculated on 6-well Transwell polyester membranes, where each well was separated by polyester membranes into two lumens with upper lumen being the apical (AP) side and lower lumen being the basolateral (BL) side. Specifically, 1.0 mL resuspended cells and 2.0 mL complete medium were placed in the AP side and BL side, respectively. The Transwell plate was placed in an incubator at 37 °C with 5 % CO_2. The medium was replaced at intervals of 1 d, and then daily a week later until differentiation from the cell monolayer model was complete.

2.4. Assessment of Caco-2 cell monolayer model

2.4.1. Morphologic observations

An inverted optical microscope (AE2000, Motic China Group Co., Ltd., Fujian, China) was utilized to observe the morphology of Caco-2 cells cultured on Transwell plates at 3, 6, 9, 15, 18, and 21 days.

2.4.2. Determination of phenol red apparent permeability coefficient

Phenol red is a small, water-soluble molecule that cannot easily pass through the membranes of Caco-2 cells and can thus be used to evaluate their integrity. The phenol red apparent permeability coefficient (P_{app}) of cells cultured for 3, 6, 9, 12, 15, 18, and 21 days was determined. Specifically, the medium in the Transwell plate was replaced with complete medium without phenol red, which was removed after 30 min of incubation. Then, 1.5 mL of 5 μg/mL HBSS with phenol red and 2.5 mL HBSS were added on AP side and BL side, respectively. After incubating for 60 min, the transfer solution was gathered from BL side to determine absorbance at 560 nm using a microplate reader (SpectraMax 190; Molecular Devices, San Jose, CA, USA). The phenol red flux (Q_{BL}) and P_{app} were calculated using Eqs. (1) and (2) below, respectively:

$$Q_{BL}\ (\mu g) = V_{BL} \times C_0 \times \frac{A_{BL} - A_0}{A_1 - A_0} \quad (1)$$

$$P_{app}\ (\mathrm{cm/s}) = \frac{dQ_{BL}}{dt} \times \frac{1}{S} \times \frac{1}{C_0} \quad (2)$$

where V_{BL} is the total volume on the BL side (2.5 mL); A_{BL} the absorbance value of the transfer solution; A_0 the absorbance value of HBSS; A_1 the absorbance value of HBSS with phenol red; C_0 the concentration of HBSS with phenol red (5 μg/mL); dQ_{BL}/dt the phenol red transmittance per unit time (μg/s); S the monolayer cell surface area (4.5 cm^2).

2.4.3. Measurement of alkaline phosphatase activity

The AKP assay was performed on the basis of He, Wang, and Moreau (2022). Specifically, after culturing in Transwell plates for 3, 6, 9, 12, 15, 18, and 21 days, the Caco-2 cells were rinsed 2–3 times by HBSS. Subsequently, 1.5 mL and 2.5 mL HBSS were added on AP side and BL side, respectively, where after the plates were placed in the incubator for 20 min, media were gathered from AP and BL sides, centrifuged at 8000 ×*g* for 5 min. AKP activity was then measured with the relevant kit.

2.5. Cell viability test

The influences of DS on Caco-2 cells viabilities were measured by CCK-8 test (Yuan, Zhang, Jia, Xie, & Shen, 2020). Caco-2 cells (1×10^5/mL) were cultured in 96-well plates at 5 % CO_2 and 37 °C for 24 h. The DS (25, 50, 100, 200, 300, 400, 500, and 600 μg/mL) was supplemented and cultured for 24 h. The medium was discarded, and DMEM containing 10 % CCK-8 was supplemented and cultured at 37 °C for 120

min. The absorbance (A) was determined at 450 nm, and cell viability calculated using Eq. (3) below:

$$\text{Cell survival rate } (\%) = \frac{A_1 - A_0}{A_2 - A_0} \times 100 \quad (3)$$

where A_0 is the absorbance of CCK-8; A_1 the absorbance of the solution with DS and CCK-8; A_2 the absorbance of the solution with CCK-8 only.

2.6. Measurement of polyphenol content

The polyphenol content of the transfer solution was determined according to Wang et al. (2021) with slight modifications. Specifically, 100 μL transfer solution was combined in an equal volume of Folin–Ciocalteu reagent and 150 μL Na_2CO_3 (10 %). After reacting in darkness for 1 h, the absorbance was measured at 765 nm. And polyphenol content (μg/mL) in the transfer solution was computed using the gallic acid standard curve ($y = 0.0329\times + 0.0474$, $R^2 = 0.99969$).

2.7. Determination of transport conditions for the digestion samples

The transfer test was performed following Xiang et al. (2020) with slight modifications. HBSS was used to configure DS solution (50, 100, 200, and 400 μg/mL). Subsequently, 1.5 mL DS solution was added to the AP side, and 2.5 mL HBSS buffer to the BL side of the Caco-2 cell monolayer. The Transwell plate was maintained at 37 °C, and aliquots were withdrawn from the BL side HBSS compartment at 60, 180, and 300 min to determine polyphenol content, P_{app}, and translocation rate. The P_{app} was calculated using Eq. (2), and translocation rate was calculated using Eq. (4) below:

$$\text{Translocation rate } (\%) = \frac{Q_2}{Q_1} \times 100 \quad (4)$$

where Q_1 is the polyphenol content in the BL side (μg/mL); Q_2 the polyphenol content in DS at different concentrations (μg/mL).

2.8. Bidirectional transport of digestion samples

Bidirectional translocation assays were carried out with Caco-2 cell monolayer model from AP to BL side (AP → BL) and from BL to AP side (BL → AP). DS (100 μg/mL) was added to AP and BL sides each and cultured for 180 min, and the transport solutions from AP → BL (TSB) and from BL → AP (TSA) were collected. Subsequently, the lyophilized DS, TSB and TSA were dissolved in 70 % methanol aqueous internal standard extraction solution respectively, and sequentially vortexed for 15 min, sonicated in an ice-water bath for 10 min, centrifuged at 12000 rpm for 3 min, and then filtered through 0.22 μm microporous filtration membrane. The supernatants were analyzed using UPLC-ESI-MS/MS. Polyphenol substance efflux ratio *(ER)* was computed according to Eq. (5) below, with reference to Yao, Xu, Ju, Li, and Wang (2020):

$$ER = \frac{P_{app(BL\rightarrow AP)}}{P_{app(AP\rightarrow BL)}} \quad (5)$$

where $P_{app(BL\rightarrow AP)}$ is the apparent permeability coefficient (cm/s) for BL → AP; $P_{app(AP\rightarrow BL)}$ the apparent permeability coefficient (cm/s) for AP → BL.

2.9. UPLC-ESI-MS/MS analyses

Metabolite analyses were performed using an ExionLC AD Ultra Performance Liquid Chromatography system (AB Sciex, Framingham, MA, USA) coupled with a QTRAP 4500 Tandem mass spectrometer (AB Sciex). An Agilent SB-C18 column (1.8 μm, 2.1 mm × 100 mm) was used. Reagents A comprised a 0.1 % formic acid aqueous solution, whereas reagent B was composed of a 0.1 % formic acid and acetonitrile solution. The following parameters were used: flow rate, 0.35 mL/min; column temperature, 40 °C; injection volume, 2 μL. The elution gradient was as follows: 0 min, 5 % B; 0–9 min, 5–95 % B; 9–10 min, 95 % B; 10.00–11.10 min, 95–5 % B; 11.10–14 min, 5 % B. The mass spectrometer was operated with a positive ion spray voltage of 5500 V and negative ion spray voltage of −4500 V. The ion source gas I was set to 50 psi, gas II to 60 psi, curtain gas to 25 psi, and the collision-induced ionization parameter set to high. The scanning mode was MRM, with collision gas (nitrogen) as the medium.

2.10. Data and statistical analyses

Graphs were plotted using Origin 2022 (Origin Lab, Northampton, MA, USA) and Microsoft Excel 2016 (Microsoft, Redmond, WA, USA). Statistical significance was determined using IBM SPSS Statistics 27 (IBM, Chicago, IL, USA). Significance was defined as $p < 0.05$. The MS data were analyzed and plotted using the Metware metabolic platform (https://cloud.metware.cn/#/user/login) and Simca 14.1 software (Umetrics, Umea, Sweden). All data are presented as mean ± standard deviation ($n = 3$).

3. Results and discussion

3.1. Modeling of the Caco-2 cell monolayer

3.1.1. Morphology of Caco-2 cells

As illustrated in Fig. 1, the Caco-2 cells were round and sparsely distributed at day 3. Then, the cells slowly fused and gradually became tightly connected at day 9, showing good growth. At days 15 and 18, some gaps between the cells were observed; however, they were densely arranged, with distinct borders and no overlap. At day 21, the Caco-2 cells were tightly connected as a whole, with no gaps, forming a complete cell monolayer. These observations were similar to those on the cell morphology described by Xiang et al. (2020) after 22 days of culture, suggesting that the Caco-2 cell monolayer model was developed with success.

3.1.2. Apparent permeability coefficient of phenol red

Phenol red is typically not metabolized or transported to the gut. Therefore, completeness of the Caco-2 cell monolayer model can be confirmed by assessing the phenol red Q_{BL} and P_{app}. As shown in Table 1 and Fig. 2a, both the Q_{BL} and P_{app} of Caco-2 cells gradually decreased with the prolongation of culture time, indicating that cells became more closely packed. After culturing for 15 days, the Q_{BL} and P_{app} were measured as 0.49 ± 0.21 μg and (0.61 ± 0.26) × 10^{-5} cm/s, respectively. And after culturing for 18 and 21 days, the P_{app} in Caco-2 cell monolayers was stabilized at around 0.45 × 10^{-5} cm/s. These findings demonstrated that phenol red leakage from AP → BL was minimal, suggesting that the integrity of Caco-2 cell monolayer model was good and was successfully constructed (Chen et al., 2021).

3.1.3. Alkaline phosphatase activity

Caco-2 cells can differentiate into brush borders, analogous to how small intestinal epithelial cells can, and produce AKP and other enzymes. AKP plays an important role in small intestinal digestion; its amount in Transwell plates is focused on the AP side and increases with cell differentiation (Abramov et al., 2021). In this work, AKP was utilized to assess the polarization degree of Caco-2 cells, and its activity in the AP and BL sides is shown in Fig. 2b. With prolongation in cell culture time, the AKP activity on both sides progressively improved; AKP activity on the AP side obviously increased, whereas that on the BL side slowly increased, which was similar to the findings reported by Zhang et al. (2022). When Caco-2 cells were cultured for 15, 18, and 21 days, AKP activity on the AP side was 2.12, 4.08, and 4.09 times greater from the BL side, respectively. After 21 days of incubation, AKP activity on the AP side was more than four-fold greater from BL side, and Caco-2 cells showed clear and stable polar differentiation. Hence, the Caco-2 cell

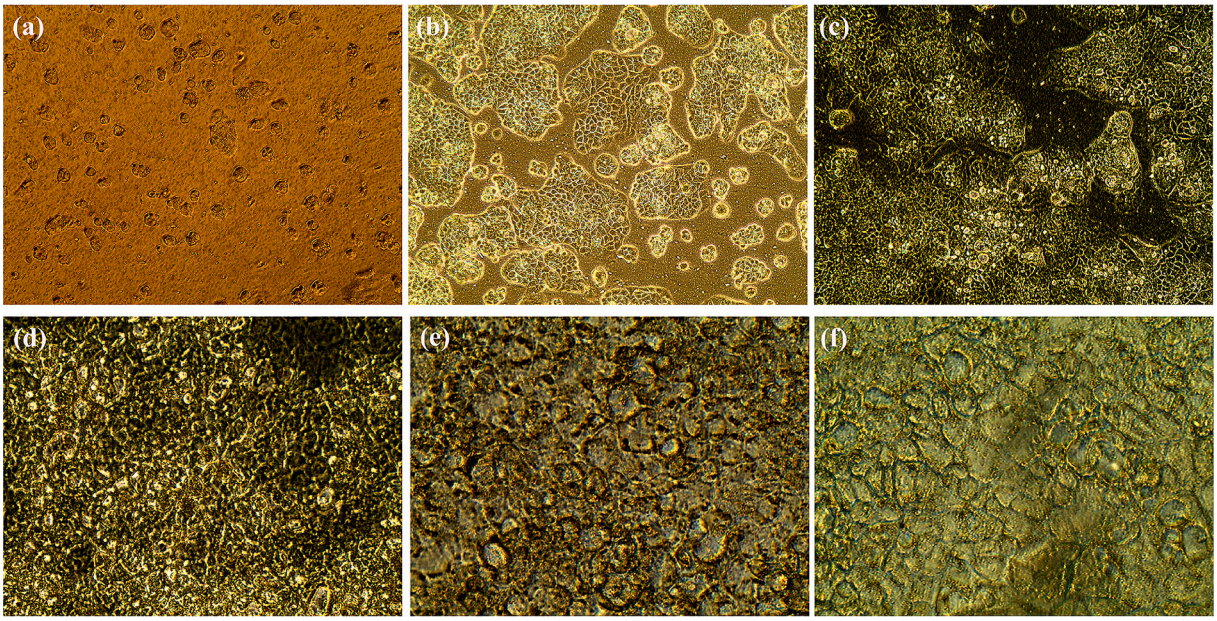

Fig. 1. Morphological observation of cells at (a) 3, (b) 6, (c) 9, (d) 15, (e) 18, and (f) 21 days.

Table 1
Phenol red flux (Q_{BL}) in Caco-2 cells at various times.

Cell culture time (day)	Q_{BL} (μg)
3	4.18 ± 0.43^{a}
6	1.94 ± 0.70^{b}
9	1.36 ± 0.44^{bc}
12	0.88 ± 0.15^{cd}
15	0.49 ± 0.21^{d}
18	0.40 ± 0.09^{d}
21	0.37 ± 0.07^{d}

Note: Values represented by different lowercase letters show significantly different ($p < 0.05$, $n = 3$).

monolayer model was further verified as suitable to subsequent experiments.

3.2. Cell viability

CCK-8 method was used to identify the safe concentration range of DS in Caco-2 cell monolayer model. As indicated in Fig. 2c, the results showed that cell viability was more than 76.50 ± 10.38 % in the range of 12.5–400 μg/mL of DS, without significantly different from blank group ($p > 0.05$). At 500 μg/mL, the cell survival ratio was lower than 50 %, remarkably different with blank group ($p < 0.05$), showing a significant cell toxicity impact at this concentration. Taken together, higher concentrations of DS resulted in decreased cell survival, whereas concentrations of 12.5–400 μg/mL were feasible for transporter studies.

3.3. Effect of different concentration and transit time on polyphenol transport

Polyphenol uptake and transit through Caco-2 cell monolayer model are affected by polyphenol content and transit time (Fang et al., 2017). The change in polyphenol content of different concentrations of DS in AP → BL with time is shown in Fig. 2d. The polyphenol content of DS at 50, 100, 200, and 400 μg/mL were 4.75 ± 0.10, 9.57 ± 0.03, 14.80 ± 0.12, and 25.72 ± 0.26 μg/mL, respectively. After 60 min, the polyphenol content of DS were detected on the BL side as 3.10 ± 0.07, 3.73 ± 0.37, 4.05 ± 0.12 and 3.54 ± 0.37 μg/mL, respectively. A slight increase in polyphenol content was observed on the BL side at 180 min, followed by a decrease at 300 min Therefore, the optimal transit time to ensure credibility of the transit study was 180 min and was applied in subsequent bidirectional transit assays.

For the AP → BL translocation of 100, 200, and 400 μg/mL DS at different times, the polyphenol contents showed little change with increasing transit time, yet they were all greater than 50 μg/mL. It was found that Caco-2 cell transit depends to some extent on cell adsorption, and the transit and uptake tend to be saturate and in dynamic equilibrium when the sample concentration reaches certain levels (Li et al., 2024). P_{app} and translocation rate can reflect the absorption ability of active ingredients in small intestine (Wu et al., 2024). To better determine the transit concentration, P_{app} and translocation rate evaluations were conducted, and the results are shown on Table 2. The P_{app} and translocation rate were both relatively large at DS concentrations of 50 and 100 μg/mL compared to 200 and 400 μg/mL. However, the transit amount of polyphenols was very low when DS was 50 μg/mL (Fig. 2d), which would affect the subsequent UPLC-ESI-MS/MS analyses of bidirectional transport products. Therefore, the DS concentration of 100 μg/mL was chosen for subsequent bidirectional transit assays.

3.4. UPLC-ESI-MS/MS analysis

3.4.1. Metabolite identification

UPLC-ESI-MS/MS was used to determine the metabolites in DS after bidirectional translocation. As shown in Fig. 3a, 400 polyphenols were identified under the positive and negative ion modes, including 169 flavonoids (42.25 %), 157 phenolic acids (39.25 %), 65 lignans and coumarins (16.25 %), 8 tannins (2 %), and 1 other compound (0.25 %). Principal component analysis was used to appraise overall metabolic discrepancies among samples. Fig. 3b shows that PC1 and PC2 were 92.8 % and 5.86 %, respectively, with a cumulative contribution of 98.66 %, suggesting a clear separation trend among DS, TSB, and TSA. To present the metabolite differences between samples more clearly, a clustered heat map was used. As illustrated in Fig. 3c, obvious differences in the DS, TSB, and TSA metabolites were noted, which were further screened and identified for differential metabolites.

Orthogonal partial least squares-discriminant analysis (OPLS-DA) is a supervised pattern-recognition multivariate statistical analysis method that reduces the dimensionality of data and facilitates screening of compounds that differ between samples (Kang et al., 2022). OPLS-DA

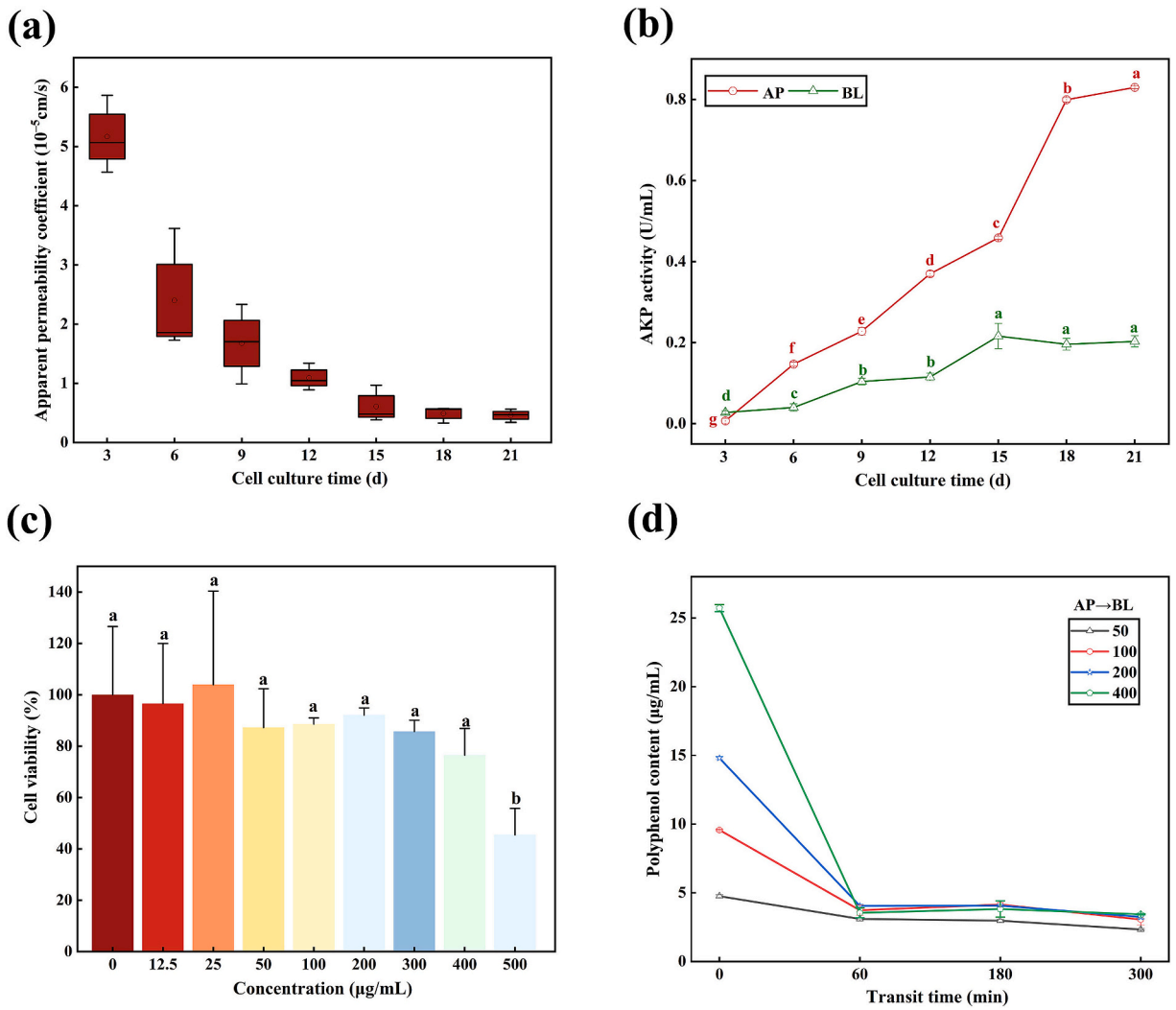

Fig. 2. (a) Apparent permeability coefficient of phenol red in Caco-2 cells; (b) alkaline phosphatase (AKP) activity on each side of the transwell plates; (c) cell survival and (d) changes in polyphenol content in digestion samples (DS) with time at different concentrations. (For interpretation of the references to colour in this figure legend, the reader is referred to the web version of this article.)

Table 2
The apparent permeability coefficient (P_{app}) and translocation rate over time at different concentrations of the digestion samples (DS).

Concentration (μg/mL)	P_{app} (× 10^{-5} cm/s)			Translocation rate (%)		
	60 min	180 min	300 min	60 min	180 min	300 min
50	15.27 ± 0.42^{Aa}	15.08 ± 1.16^{Aa}	11.07 ± 0.61^{Ab}	65.11 ± 1.60^{Aa}	65.41 ± 6.94^{Aa}	47.85 ± 1.97^{Ab}
100	9.55 ± 1.10^{Ba}	10.19 ± 0.56^{Ba}	6.87 ± 1.03^{Bb}	43.30 ± 10.59^{Ba}	45.40 ± 4.12^{Ba}	30.47 ± 3.95^{Ba}
200	6.30 ± 0.22^{Ca}	6.11 ± 0.25^{Ca}	5.36 ± 0.67^{Ca}	27.19 ± 0.72^{Ca}	26.25 ± 1.12^{Ca}	23.06 ± 3.03^{Ca}
400	3.22 ± 0.39^{Da}	2.77 ± 1.35^{Da}	3.12 ± 0.04^{Da}	13.76 ± 1.51^{Da}	15.01 ± 3.02^{Da}	13.49 ± 0.28^{Da}

Note: Different uppercase letters represent significant differences in P_{app} and translocation rate for different concentrations of DS at the same time. Different lowercase letters represent significant differences in P_{app} and translocation rate for DS at different transit times at the same concentration. Data are indicated as mean ± SD (n = 3).

score plots are shown in Fig. 3d, and the three samples could be clearly separated with $R^2X = 0.963$, $R^2Y = 0.999$, and $Q^2 = 0.97$, which are close to 1, indicating that the model has good interpretation and high predictive power. The results of the model replacement test are presented in Fig. 3e, where the intersection of the Q^2 regression line and longitudinal intercept is on the negative axis, indicating that the model was not overfitted, has high predictive ability, and can be used to analyze inter-sample variability.

3.4.2. *Differential metabolite screening and analysis*

To explore the metabolite differences of DS before and after bidirectional transit in Caco-2 cell monolayer model, differential metabolites were selected with VIP ≥ 1, $p < 0.05$, and fold change >2.0 or < 0.5 based on OPLS-DA analysis (Zeng, Lin, Liu, & Liu, 2020). The volcano plot showed nine upregulated and 248 downregulated differential metabolites for TSB vs. DS (Fig. 4a), and nine upregulated metabolites were significantly accumulated in TSB, as shown in Fig. 4d, including phenolic acids [3-(3-hydroxyphenyl)-3-hydroxypropanoic acid, 4-hydroxyphenyllactic acid, anthranilic acid, asperuloside, methyl 2,4-dihydroxyphenylacetate], flavonoids (diosmetin-7-*O*-glucuronide, hispidulin-8-C-glucoside, loquatoside), and lignans and coumarins (3,4-methylenedioxyellagic acid). Seven upregulated and 213 downregulated differential metabolites were observed in TSA vs. DS (Fig. 4b),

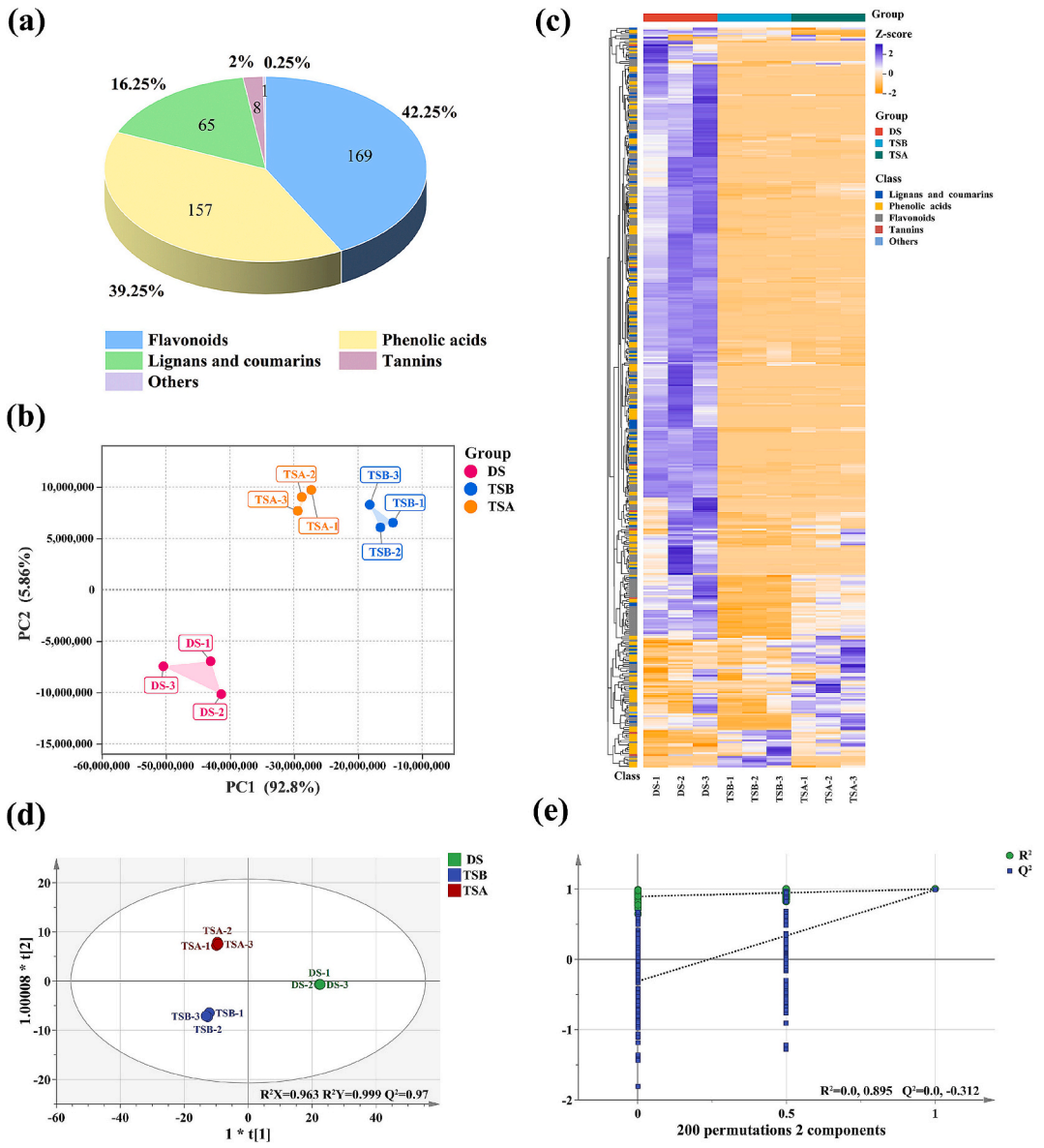

Fig. 3. Identification of metabolites in digestion samples (DS), transport solution from the apical to the basolateral side (TSB), and transport solution from the basolateral to the apical side (TSA). (a) Metabolite category; (b) principal component analysis; (c) heat map of cluster analyses; (d) orthogonal partial least squares-discriminant analysis (OPLS-DA); (e) diagram for the OPLS-DA model permutation test.

of which seven upregulated metabolites were significantly accumulated in TSA, mainly phenolic acids [2-hydroxy-3-phenylpropanoic acid, 3-(4-hydroxyphenyl)-propionic acid, asperuloside, caffeic acid, isoferulic acid, *O*-anisic acid], but also a flavonoid substance (chrysin) (Fig. 4e). These findings indicated the absorbability of phenolic acids was higher than that of flavonoids, which was consistent with the investigation of absorption and transport of polyphenols from mulberry leaves (Zhao et al., 2024).

A total of 53 differential metabolites were identified in TSA vs. TSB (Fig. 4c), of which 40 were upregulated and 13 downregulated. The 13 polyphenols likely favored the uptake and transport of AP → BL, whereas the 40 polyphenols likely favored the efflux transport of BL → AP (Fig. 4f). The DS underwent bidirectional transport and increased the abundance of some polyphenols in AP and BL sides, where the number of polyphenols was higher in the AP side. This could be due to the presence of hydrolases in AP side of Caco-2 cell monolayer, which could break down some of the structurally complex polyphenols that were transferred to the AP side into small-molecule polyphenols, thereby increasing their abundances (Wojtunik-Kulesza et al., 2020).

3.4.3. *Efflux ratio*

To further study the transport patterns of the polyphenols in DS, we analyzed the P_{app} and *ER* of 53 differential metabolites in TSA vs. TSB (Yao et al., 2020), and the results are described in Table 3. P_{app} can be used as an indicator of the uptake of polyphenolic substances by the human small intestine as determined by AP → BL and BL → AP (Rocchetti et al., 2024); $P_{app} < 1 \times 10^{-6}$ cm/s indicates a poor uptake, P_{app} between 1×10^{-6} cm/s and 10×10^{-6} cm/s a moderate uptake, and $P_{app} > 1 \times 10^{-5}$ cm/s a high uptake (Yee, 1997). Forty-three polyphenols with a $P_{app(AP \rightarrow BL)}$ and $P_{app(BL \rightarrow AP)}$ higher than 1×10^{-6} cm/s were identified, showing that these were moderately absorbed. The transported polyphenols were dominated by flavonoids, and the $P_{app\ (AP \rightarrow BL)}$ of flavonoids were generally lower than those of phenolic acids, suggesting that the absorption rate of flavonoids was lower than that of phenolic acids, which might be related to the complex structure of flavonoids (Zhao et al., 2020). In addition, 10 polyphenols, including isoferulic acid, hispidulin-8-C-glucoside, diosmetin-7-*O*-glucuronide, *O*-anisic acid, 3-(3-hydroxyphenyl)-3-hydroxypropanoic acid, methyl 2,4-dihydroxyphenylacetate, ferulic acid, 4-hydroxyphenyllactic acid, 7-

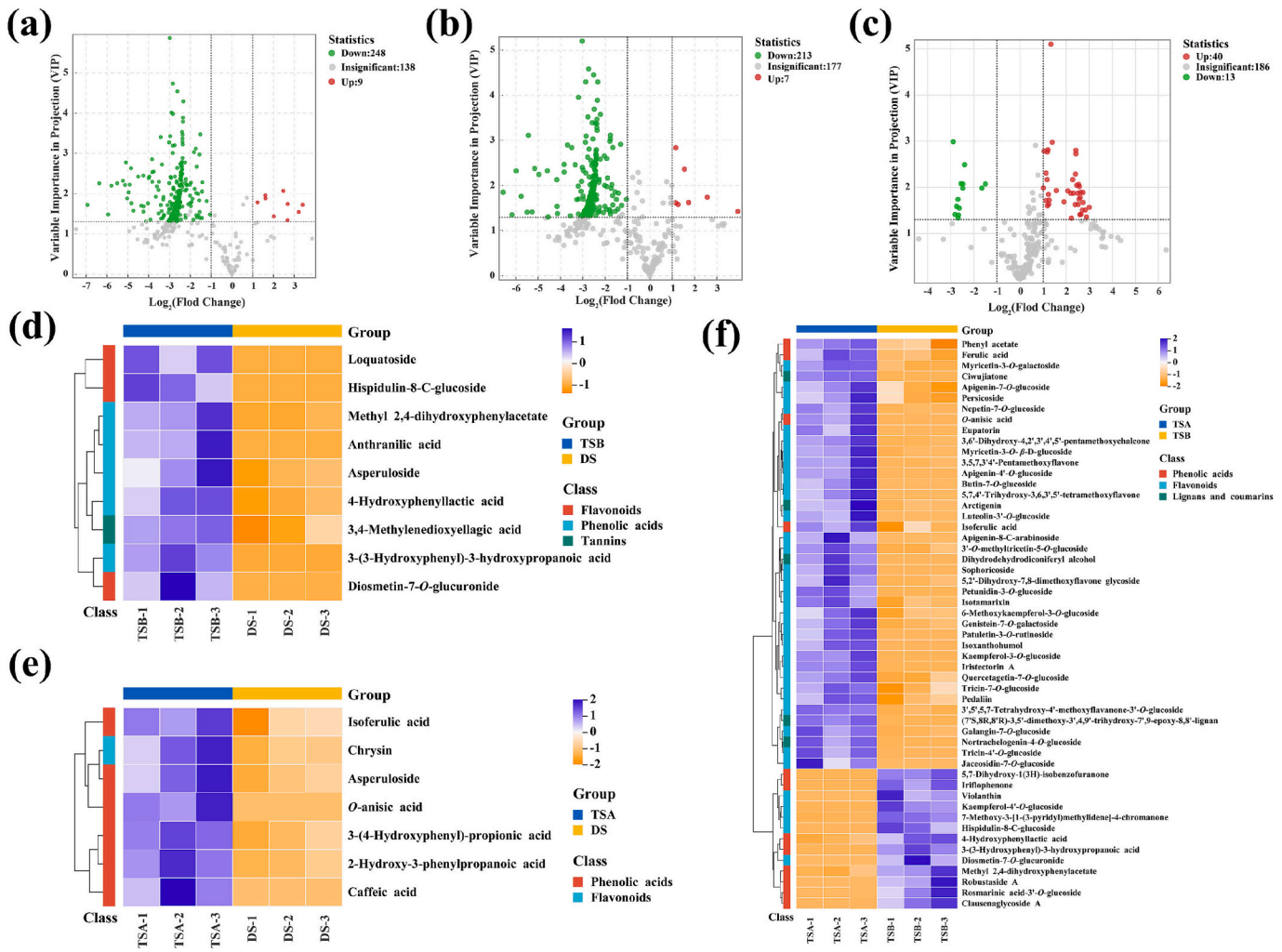

Fig. 4. Metabolites identified after differential analyses of transport solution from the apical to the basolateral side (TSB) vs. digestion samples (DS), transport solution from the basolateral to the apical side (TSA) vs. DS, and TSA vs. TSB. Volcano map of differential metabolites in (a) TSB vs. DS, (b) TSA vs. DS, and (c) TSA vs. TSB; (d–f) heat maps of the nine upregulated compounds in TSA vs. DS; (e) seven upregulated compounds in TSB vs. DS, and (f) 40 upregulated and 13 downregulated compounds in TSA vs. TSB.

methoxy-3-[1-(3-pyridyl)methylidene]-4-chromanone, and robustaside A, showed a $P_{app} > 1 \times 10^{-5}$ cm/s in AP → BL lateral transport, indicating high permeability and 70 % − 100 % uptake (Xiang et al., 2020). The 35 polyphenols, such as isotamarixin, arctigenin, and persicoside, showed similarly high permeability in the BL → AP lateral transporter. Previous studies showed that polyphenols, such as methyl 2,4-dihydroxyphenylacetate, isoferulic acid, ferulic acid, isotamarixin, arctigenin, and persicoside, have significant hypoglycemic, antioxidant, anti-inflammatory, antidepressant, anti-tumor, and antibacterial effects (Arfin, Siddiqui, Naeem, & Moin, 2018; Dong & Huang, 2022; He et al., 2018; Li et al., 2023; Sadeghi, Zolfaghari, Senatore, & Lanzotti, 2013; Yang et al., 2024), especially ferulic acid, and arctigenin retains a certain degree of antioxidant and anti-inflammatory effect after transport (Poquet, Clifford, & Williamson, 2008; Shin, Jung, Back, Do, & Shon, 2015). Additionally, 40 polyphenols with $P_{app(BL→AP)}$ higher than $P_{app(AP→BL)}$ were observed, suggesting that polyphenols could prefer BL → AP efflux during bidirectional transit in Caco-2 cell monolayer model.

ER is a ratio between $P_{app(BL→AP)}$ and $P_{app(AP→BL)}$, which can be applied for determining the transporter pathway and ratio of different transporters of a substance in Caco-2 cells monolayer model (Elendran, Muniyandy, Lee, & Palanisamy, 2018). With an $ER < 1.5$, polyphenols undergo passive diffusion, whereas an $ER > 1.5$ indicates the need for active transport, requiring the involvement of transporter proteins (Xiao et al., 2024). As shown in Table 3, 40 polyphenols with an $ER > 1.5$ were identified, suggesting that these polyphenols may be involve in active transport that requires the function of transporter proteins and energy; literature reports that isoxanthohumol and ferulic acid are translocated via active transport (Chen et al., 2021). Thirteen polyphenols with an $ER < 1.5$ were observed, which may be absorbed and transported via passive diffusion. The transit for polyphenolic compounds in DS in Caco-2 cell monolayer model evidently includes passive and active modes of transport, with active transport being predominant. This may be because the polyphenols in DS have complex groups that cannot pass directly through the cell and thus rely on transporter proteins and energy for uptake (Woottisin, Sukprasert, Kulsirirat, Tharavanij, & Sathirakul, 2022).

4. Conclusion

This study was conducted to identify the metabolites involved in bidirectional transit in DS using Caco-2 cell monolayer model and UPLC-ESI-MS/MS. The results showed that 400 metabolites, including 157 phenolic acids, 169 flavonoids, 65 lignans and coumarins, 8 tannins, and 1 other compound, were identified in DS, TSB, and TSA, and that these metabolites were differentiated among the samples. TSA vs. TSB contained 53 different polyphenols, 43 of which exhibited moderate

Table 3
53 polyphenol compounds apparent permeability coefficient (P_{app}) and efflux ratio (*ER*) for bidirectional transportation.

Class	Compounds	Formula	Peak area			$P_{app\ (AP→BL)}$ (10^{-6} cm/s)	$P_{app\ (BL→AP)}$ (10^{-6} cm/s)	*ER*
			DS	TSB	TSA			
Flavonoids	Eupatorin	$C_{18}H_{16}O_7$	10,186.25	1074.35	8547.33	2.17	17.30	7.97
	Jaceosidin-7-*O*-glucoside	$C_{23}H_{24}O_{12}$	60,082.25	5801.30	42,595.25	1.99	14.59	7.33
	5,7,4′-Trihydroxy-3,6,3′,5′-tetramethoxyflavone	$C_{19}H_{18}O_9$	117,706.75	18,554.35	132,106.50	3.24	23.10	7.13
	Patuletin-3-*O*-rutinoside	$C_{28}H_{32}O_{17}$	180,809.10	5931.22	39,367.12	0.67	4.48	6.69
	Isoxanthohumol	$C_{21}H_{22}O_5$	26,550.00	4516.00	29,934.25	3.50	23.20	6.63
	Butin-7-*O*-glucoside	$C_{21}H_{22}O_{10}$	126,178.16	6177.84	40,059.73	1.01	6.53	6.47
	Luteolin-3′-*O*-glucoside	$C_{21}H_{20}O_{11}$	204,053.00	7069.26	44,149.85	0.71	4.45	6.27
	Tricin-4′-*O*-glucoside	$C_{23}H_{24}O_{12}$	50,320.00	7610.97	46,928.20	3.11	19.19	6.17
	Sophoricoside	$C_{21}H_{20}O_{10}$	125,525.05	9913.55	60,337.67	1.63	9.89	6.07
	Apigenin-8-C-arabinoside	$C_{20}H_{18}O_9$	24,568.25	2211.50	13,338.50	1.85	11.17	6.04
	Petunidin-3-*O*-glucoside	$C_{22}H_{23}O_{12}$	100,893.33	2967.48	17,316.11	0.61	3.53	5.79
	Apigenin-4′-*O*-glucoside	$C_{21}H_{20}O_{10}$	132,449.50	9316.70	53,732.50	1.45	8.35	5.76
	Astragalin	$C_{21}H_{20}O_{11}$	102,451.90	3864.25	21,227.28	0.78	4.26	5.46
	Iristectorin A	$C_{23}H_{24}O_{12}$	62,366.83	6245.50	33,155.33	2.06	10.94	5.31
	3,5,7,3′4′-Pentamethoxyflavone	$C_{20}H_{20}O_7$	157,030.75	39,619.50	208,357.25	5.19	27.30	5.26
	3,6′-Dihydroxy-4,2′,3′,4′,5′-pentamethoxychalcone	$C_{20}H_{22}O_8$	95,961.00	25,055.92	124,189.92	5.37	26.63	4.96
	Galangin-7-*O*-glucoside	$C_{21}H_{20}O_{10}$	107,042.70	13,621.69	66,313.79	2.62	12.75	4.87
	Cosmosiin	$C_{21}H_{20}O_{10}$	106,262.46	11,120.37	51,040.42	2.15	9.88	4.60
	Genistein-7-*O*-galactoside	$C_{21}H_{20}O_{10}$	94,283.66	13,146.17	55,454.21	2.87	12.10	4.22
	Persicoside	$C_{23}H_{26}O_{11}$	153,136.32	22,650.62	84,948.15	3.04	11.41	3.75
	Tricin-7-*O*-glucoside	$C_{23}H_{24}O_{12}$	64,930.67	16,194.08	48,266.34	5.13	15.30	2.98
	Myricetin-3-*O*-galactoside	$C_{21}H_{20}O_{13}$	419,190.00	138,407.92	363,885.33	6.79	17.86	2.63
	3′,5′,5,7-Tetrahydroxy-4′-methoxyflavanone-3′-*O*-glucoside	$C_{22}H_{24}O_{12}$	319,672.58	90,803.42	230,635.83	5.84	14.85	2.54
	6-Methoxykaempferol-3-*O*-glucoside	$C_{22}H_{22}O_{12}$	13,760,639.27	3,985,405.53	9,551,299.66	5.96	14.28	2.40
	Myricetin-3-*O*-β-D-glucoside	$C_{21}H_{20}O_{13}$	413,225.17	141,033.17	333,469.17	7.02	16.60	2.36
	Nepitrin	$C_{22}H_{22}O_{12}$	12,979,293.24	4,411,376.79	1,035,916.12	6.99	16.42	2.35
	3′-*O*-Methyltricetin-5-*O*-glucoside	$C_{22}H_{22}O_{12}$	11,253,621.60	3,377,503.11	780,122.16	6.18	14.27	2.31
	5,2′-Dihydroxy-7,8-dimethoxyflavone glycoside	$C_{23}H_{24}O_{11}$	943,877.79	140,028.50	319,602.25	3.05	6.97	2.29
	Quercetagitrin	$C_{21}H_{20}O_{13}$	398,003.21	138,709.17	315,943.67	7.17	16.33	2.28
	Pedaliin	$C_{22}H_{22}O_{12}$	12,566,691.22	3,892,430.43	8,491,000.13	6.37	13.90	2.18
	Isotamarixin	$C_{22}H_{22}O_{12}$	15,944,894.29	5,373,553.94	11,099,858.66	6.93	14.32	2.07
	Kaempferol-4′-*O*-glucoside	$C_{21}H_{20}O_{11}$	210,163.99	18,520.69	3323.36	1.81	0.33	0.18
	Violanthin	$C_{27}H_{30}O_{14}$	94,907.18	15,179.32	2452.40	3.29	0.53	0.16
	Diosmetin-7-*O*-glucuronide	$C_{22}H_{20}O_{12}$	4142.30	26,494.75	4142.30	131.61	20.58	0.16
	Hispidulin-8-C-glucoside	$C_{22}H_{22}O_{11}$	3824.00	24,550.33	3824.00	132.10	20.58	0.16
	7-Methoxy-3-[1-(3-pyridyl)methylidene]-4-chromanone	$C_{16}H_{13}NO_3$	830,240.11	842,133.28	113,574.30	20.87	2.81	0.13
	O-anisic acid	$C_8H_8O_3$	3054.55	3054.55	18,079.51	20.58	121.79	5.92
	Ferulic acid	$C_{10}H_{10}O_4$	93,745.71	79,124.62	178,424.28	17.37	39.16	2.25
	Phenyl acetate	$C_8H_8O_2$	218,517.30	94,454.52	206,417.22	8.89	19.44	2.19
	Isoferulic acid	$C_{10}H_{10}O_4$	70,481.96	83,955.58	169,431.00	24.51	49.46	2.02
	Methyl 2,4-dihydroxyphenylacetate	$C_9H_{10}O_4$	109,580.46	334,121.87	118,309.72	62.74	22.22	0.35
	4-Hydroxyphenyllactic acid	$C_9H_{10}O_4$	130,658.32	397,105.72	126,495.57	62.54	19.92	0.32
Phenolic acids	5,7-Dihydroxy-1(3H)-isobenzofuranone	$C_8H_6O_4$	608,970.19	134,649.98	25,408.80	4.55	0.86	0.19
	3-(3-Hydroxyphenyl)-3-hydroxypropanoic acid	$C_9H_{10}O_4$	1428.60	7950.92	1428.60	114.52	20.58	0.18
	Iriflophenone	$C_{13}H_{10}O_5$	73,963.50	9689.50	1648.70	2.70	0.46	0.17
	Robustaside A	$C_{21}H_{22}O_9$	32,629.61	18,380.67	2899.45	11.59	1.83	0.16
	Clausenaglycoside A	$C_{17}H_{26}O_8$	20,310.17	7604.42	1134.90	7.70	1.15	0.15
	Rosmarinic acid-3′-*O*-glucoside	$C_{24}H_{26}O_{13}$	141,305.74	22,974.35	3264.73	3.35	0.48	0.14
	Nortrachelogenin-4-*O*-glucoside	$C_{26}H_{32}O_{12}$	451,566.29	12,888.20	76,841.95	0.59	3.50	5.93
	Dihydrodehydrodiconiferyl alcohol	$C_{20}H_{24}O_6$	28,511.17	4496.32	25,416.36	3.24	18.34	5.66
Lignans and coumarins	(7′*S*,8*R*,8′*R*)-3,5′-Dimethoxy-3′,4,9′-trihydroxy-7′,9-epoxy-8,8′-lignan	$C_{20}H_{24}O_6$	33,808.09	4172.16	22,365.22	2.54	13.61	5.36
	Ciwujiatone	$C_{22}H_{26}O_9$	28,010.31	3792.26	20,284.47	2.79	14.90	5.34
	Arctigenin	$C_{21}H_{24}O_6$	155,823.17	40,631.42	190,697.92	5.37	25.18	4.69

absorption and were dominated by flavonoids. Moreover, polyphenol translocation was mainly active transport. This study provides a foundation for further exploration of the metabolism of phenolic compounds in *C. fascicularis*, as well as for the development of CFPs into functional products or orally consumed drugs.

CRediT authorship contribution statement

Shengjiang Duan: Writing – original draft, Methodology, Investigation, Formal analysis, Data curation, Conceptualization. **Hao Zheng:** Methodology, Data curation. **Junrong Tang:** Resources. **Huan Kan:** Supervision, Conceptualization. **Changwei Cao:** Validation, Supervision, Formal analysis. **Zhijiao Shi:** Writing – review & editing, Formal analysis, Data curation, Conceptualization. **Yun Liu:** Writing – review & editing, Validation, Resources, Funding acquisition.

Declaration of competing interest

The authors declare that they have no known competing financial interests or personal relationships that could have appeared to influence

the work reported in this paper.

Acknowledgments

This work was supported by Yunnan Fundamental Research Projects (202201AT070050), and Youth Talents Special Project of Yunnan Province "Xingdian Talents Support Program" (XDYC-QNRC-2022-0222).

Data availability

Data will be made available on request.

References

Abramov, V. M., Kosarev, I. V., Priputnevich, T. V., Machulin, A. V., Abashina, T. N., Chikileva, I. O., … A. V.. (2021). S-layer protein 2 of vaginal *Lactobacillus crispatus* 2029 enhances growth, differentiation, VEGF production and barrier functions in intestinal epithelial cell line Caco-2. *International Journal of Biological Macromolecules, 189*, 410–419. https://doi.org/10.1016/j.ijbiomac.2021.08.150

Arfin, S., Siddiqui, G. A., Naeem, A., & Moin, S. (2018). Inhibition of advanced glycation end products by isoferulic acid and its free radical scavenging capacity: An in vitro and molecular docking study. *International Journal of Biological Macromolecules, 118*, 1479–1487. https://doi.org/10.1016/j.ijbiomac.2018.06.182

Brodkorb, A., Egger, L., Alminger, M., Alvito, P., Assunção, R., Ballance, S., Recio, & I.. (2019). INFOGEST static *in vitro* simulation of gastrointestinal food digestion. *Nature Protocols, 14*(4), 991–1014. https://doi.org/10.1038/s41596-018-0119-1

Chen, C., Li, T., Chen, Z. X., Wang, L., & Luo, X. H. (2020). Absorption rates and mechanisms of avenanthramides in a Caco-2 cell model and their antioxidant activity during absorption. *Journal of Agricultural and Food Chemistry, 68*(8), 2347–2356. https://doi.org/10.1021/acs.jafc.9b06576

Chen, Y. H., Zhang, H., Fan, W. Y., Mats, L. L., Liu, R. H., Deng, Z. Y., & Tsao, R. (2021). Anti-inflammatory effect and cellular transport mechanism of phenolics from common bean (*Phaseolus vulga* L.) milk and yogurts in Caco-2 mono- and Caco-2/EA. hy926 co-culture models. *Journal of Agricultural and Food Chemistry, 69*(5), 1513–1523. https://doi.org/10.1021/acs.jafc.0c06934

Dong, X. Y., & Huang, R. (2022). Ferulic acid: An extraordinarily neuroprotective phenolic acid with anti-depressive properties. *Phytomedicine, 105*, Article 154355. https://doi.org/10.1016/j.phymed.2022.154355

Elendran, S., Muniyandy, S., Lee, W. W., & Palanisamy, U. D. (2018). Permeability of the ellagitannin geraniin and its metabolites in a human colon adenocarcinoma Caco-2 cell culture model. *Food & Function, 10*(2), 602–615. https://doi.org/10.1039/c8fo01927d

Fang, Y. J., Liang, Q. F., Liu, K. Y., Qaiser, S., Pan, S. Y., & Xu, X. Y. (2017). Structure characteristics for intestinal uptake of flavonoids in Caco-2 cells. *Food Research International, 105*, 353–360. https://doi.org/10.1016/j.foodres.2017.11.045

Faralli, A., Shekarforoush, E., Ajalloueian, F., Mendes, A., & Chronakis, I. S. (2018). *In vitro* permeability enhancement of curcumin across Caco-2 cells monolayers using electrospun xanthan-chitosan nanofibers. *Carbohydrate Polymers, 206*, 38–47. https://doi.org/10.1016/j.carbpol.2018.10.073

Gao, M. Z., Peng, X. W., Tang, J. R., Deng, J., Wang, F., Zhang, Y. J., … Liu, Y. (2022). Anti-inflammatory effects of *Camellia fascicularis* polyphenols via attenuation of NF-κB and MAPK pathways in LPS-induced THP-1 macrophages. *Journal of Inflammation Research, 15*, 851–864. https://doi.org/10.2147/JIR.S349981

He, B., Wang, Z. G., & Moreau, R. (2022). Chylomicron production is repressed by RPTOR knockdown, *R*-α-lipoic acid and 4-phenylbutyric acid in human enterocyte-like Caco-2 cells. *The Journal of Nutritional Biochemistry, 108*, Article 109087. https://doi.org/10.1016/j.jnutbio.2022.109087

He, H. Y., Fan, Q. M., Cai, T. T., Huang, W., Xie, X. Z., Wen, Y. Y., & Shi, Z. (2018). Molecular mechanisms of the action of Arctigenin in cancer. *Biomedicine & Pharmacotherapy, 108*, 403–407. https://doi.org/10.1016/j.biopha.2018.08.158

Hlel, T. B., Borges, T., Rueda, A., Smaali, I., Marzouki, M. N., & Seiquer, I. (2018). Polyphenols bioaccessibility and bioavailability assessment in ipecac infusion using a combined assay of simulated *in vitro* digestion and Caco-2 cell model. *International Journal of Food Science and Technology, 54*(5), 1566–1575. https://doi.org/10.1111/ijfs.14023

Kang, C. D., Zhang, Y. Y., Zhang, M. Y., Qi, J., Zhao, W. T., Gu, J., … Li, Y. Y. (2022). Screening of specific quantitative peptides of beef by LC-MS/MS coupled with OPLS-DA. *Food Chemistry, 387*, Article 132932. https://doi.org/10.1016/j.foodchem.2022.132932

Li, L., Xia, M. J., Yang, L. N., He, Y. T., Liu, H., Xie, M. X., & Yu, M. (2024). The decreased interface tension increased the transmembrane transport of soy hull polysaccharide-derived SCFAs in the Caco-2 cells. *International Journal of Biological Macromolecules, 266*, Article 131261. https://doi.org/10.1016/j.ijbiomac.2024.131261

Li, Z. Y., Jiang, H., Tang, J. R., Jiang, X. M., Zhang, L. F., & Qin, Y. (2023). Integrated physiological, transcriptomic, and metabolomic analyses reveal that low-nitrogen conditions improve the accumulation of flavonoids in snow chrysanthemum. *Industrial Crops and Products, 197*, Article 116574. https://doi.org/10.1016/j.indcrop.2023.116574

Liu, Y., Kan, H., Fan, F. Y., Tang, J. R., Zhang, Y. J., & Zhao, P. (2019). Microwave-assisted extraction and antioxidant activities of polyphenols from *Camellia fascicularis* leaves. *Current Topics in Nutraceutical Research, 17*(2), 164–173. https://doi.org/10.37290/ctnr2641-452x.17:164-171

Peng, X. W., Hu, X., Zhang, Y. J., Xu, H., Tang, J. R., Zhang, G. L., … Liu, Y. (2022). Extraction, characterization, antioxidant and anti-tumor activities of polysaccharides from *Camellia fascicularis* leaves. *International Journal of Biological Macromolecules, 222*, 373–384. https://doi.org/10.1016/j.ijbiomac.2022.09.176

Poquet, L., Clifford, M. N., & Williamson, G. (2008). Transport and metabolism of ferulic acid through the colonic epithelium. *Drug Metabolism and Disposition, 36*(1), 190–197. https://doi.org/10.1124/dmd.107.017558

Rocchetti, G., Chiodelli, G., Giuberti, G., & Lucini, L. (2018). Bioaccessibility of phenolic compounds following *in vitro* large intestine fermentation of nuts for human consumption. *Food Chemistry, 245*, 633–640. https://doi.org/10.1016/j.foodchem.2017.10.146

Rocchetti, G., Lucini, L., Gonçalves, J. E., Camps, I., dos Santos Lima, A., Granato, D., … Azevedo, L. (2024). Cellular assays combined with metabolomics highlight the dual face of phenolics: From high permeability to morphological cell damage. *Food Chemistry, 430*, Article 137081. https://doi.org/10.1016/j.foodchem.2023.137081

Sadeghi, M., Zolfaghari, B., Senatore, M., & Lanzotti, V. (2013). Spirostane, furostane and cholestane saponins from Persian leek with antifungal activity. *Food Chemistry, 141*(2), 1512–1521. https://doi.org/10.1016/j.foodchem.2013.04.009

Shin, H. S., Jung, S. Y., Back, S. Y., Do, J. R., & Shon, D. H. (2015). Arctigenin from *fructus arctii* (seed of burdock) reinforces intestinal barrier function in Caco-2 cell monolayers. *Evidence-Based Complementary and Alternative Medicine, 2015*(1), Article 368105. https://doi.org/10.1155/2015/368105

Taboada-López, M. V., Leal-Martínez, B. H., Domínguez-González, R., Bermejo-Barrera, P., Taboada-Antelo, P., & Moreda-Piñeiro, A. (2021). Caco-2 *in vitro* model of human gastrointestinal tract for studying the absorption of titanium dioxide and silver nanoparticles from seafood. *Talanta, 233*, Article 122494. https://doi.org/10.1016/j.talanta.2021.122494

Tang, J. D., Li, R. N., Wu, B. X., Tang, J. R., Kan, H., Zhao, P., … Liu, Y. (2024). Secondary metabolites with antioxidant and antimicrobial activities from *Camellia fascicularis*. *Current Issues in Molecular Biology, 46*(7), 6769–6782. https://doi.org/10.3390/cimb46070404

Wang, W., Gao, Y. T., Wei, J. W., Chen, Y. F., Liu, Q. L., & Liu, H. M. (2021). Optimization of ultrasonic cellulase-assisted extraction and antioxidant activity of natural polyphenols from passion fruit. *Molecules, 26*(9), 2494. https://doi.org/10.3390/molecules26092494

Wojtunik-Kulesza, K., Oniszczuk, A., Oniszczuk, T., Combrzyński, M., Nowakowska, D., & Matwijczuk, A. (2020). Influence of *in vitro* digestion on composition, bioaccessibility and antioxidant activity of food polyphenols–A non-systematic review. *Nutrients, 12*(5), 1401. https://doi.org/10.3390/nu12051401

Woottisin, N., Sukprasert, S., Kulsirirat, T., Tharavanij, T., & Sathirakul, K. (2022). Evaluation of the intestinal permeability of rosmarinic acid from *Thunbergia laurifolia* leaf water extract in a Caco-2 cell model. *Molecules, 27*(12), 3884. https://doi.org/10.3390/molecules27123884

Wu, S. J., Jiang, P., Zhang, X. L., Mao, C., Dai, Y. X., Zhuang, H., & Pang, Y. (2024). Understanding the transepithelial transport and transbilayer diffusion of the antihypertensive peptide Asn-Cys-Trp: Insights from Caco-2 cell monolayers and the DPPC model membrane. *Journal of Agricultural and Food Chemistry, 72*(17), 9828–9841. https://doi.org/10.1021/acs.jafc.4c0015

Xiang, Q. F., Zhang, W. J., Li, Q., Zhao, J., Feng, W. W., Zhao, T., … Chen, G. Y. (2020). Investigation of the uptake and transport of polysaccharide from se-enriched *Grifola frondosa* in Caco-2 cells model. *International Journal of Biological Macromolecules, 158*, 1330–1341. https://doi.org/10.1016/j.ijbiomac.2020.04.160

Xiao, J. J., Li, M. K., Zhang, M. Y., Dai, K. J., Ju, X. W., Liu, Y. J., … Shi, Y. H. (2024). Transport and interaction mechanism of four pesticide residues from *Chaenomeles speciosa* across Caco-2 cells. *Food Chemistry, 431*, Article 137156. https://doi.org/10.1016/j.foodchem.2023.137156

Yang, J., Dong, M. J., Fang, F., Li, Y., & Li, C. L. (2024). Effects of varied preparation processes on polyphenol-rice starch complexes, *in vitro* starch digestion, and polyphenols release. *Food Chemistry, 450*, Article 139330. https://doi.org/10.1016/j.foodchem.2024.139330

Yang, Y. F., He, J. Z., Wu, L., Jiang, Z. D., Du, X. P., Chen, F., … Ni, H. (2024). Towards understanding enhanced hypoglycemic activity of fermented bee pollen in insulin-resistant HepG2 cells by widely targeted metabolomics analysis. *Food Bioscience, 61*, Article 104667. https://doi.org/10.1016/j.fbio.2024.104667

Yao, Y. J., Xu, F. R., Ju, X. R., Li, Z. F., & Wang, L. F. (2020). Lipid-lowering effects and intestinal transport of polyphenol extract from digested buckwheat in Caco-2/HepG2 coculture models. *Journal of Agricultural and Food Chemistry, 68*(14), 4205–4214. https://doi.org/10.1021/acs.jafc.0c00321

Yee, S. (1997). *In vitro* permeability across Caco-2 cells (colonic) can predict *in vivo* (small intestinal) absorption in man—fact or myth. *Pharmaceutical Research, 14*(6), 763–766. https://doi.org/10.1023/a:1012102522787

Yuan, L. L., Zhang, F., Jia, S., Xie, J. H., & Shen, M. Y. (2020). Differences between phytosterols with different structures in regulating cholesterol synthesis, transport and metabolism in Caco-2 cells. *Journal of Functional Foods, 65*, Article 103715. https://doi.org/10.1016/j.jff.2019.103715

Zeng, C. Z., Lin, H. Y., Liu, Z. X., & Liu, Z. H. (2020). Metabolomics analysis of *Camellia sinensis* with respect to harvesting time. *Food Research International, 128*, Article 108814. https://doi.org/10.1016/j.foodres.2019.108814

Zhang, Z. D., Tao, Q., Qin, Z., Liu, X. W., Li, S. H., Bai, L. X., … Li, J. Y. (2022). Uptake and transport of naringenin and its antioxidant effects in human intestinal epithelial

Caco-2 cells. *Frontiers in Nutrition, 9*, Article 894117. https://doi.org/10.3389/fnut.2022.894117

Zhao, Q. N., Yang, J. Y., Li, J. H., Zhang, L., Yan, X. H., Yue, T. L., & Yuan, Y. H. (2024). Hypoglycemic effect and intestinal transport of phenolics-rich extract from digested mulberry leaves in Caco-2/insulin-resistant HepG2 co-culture model. *Food Research International, 175*, Article 113689. https://doi.org/10.1016/j.foodres.2023.113689

Zhao, Y. Y., Fan, Y., Wang, M., Wang, J., Cheng, J. X., Zou, J. B., … Gou, D. Y. (2020). Studies on pharmacokinetic properties and absorption mechanism of phloretin: *In vivo* and *in vitro*. *Biomedicine & Pharmacotherapy, 132*, Article 110809. https://doi.org/10.1016/j.biopha.2020.110809